



Linkage mapping reveals loci that underlie differences in *Caenorhabditis elegans* growth

Joy Nyaanga ^{1,2}, Erik C. Andersen ^{1,*}

¹Department of Molecular Biosciences, Northwestern University, Evanston, IL 60208, USA,

²Interdisciplinary Biological Sciences Program, Northwestern University, Evanston, IL 60208, USA

*Corresponding author: Department of Molecular Biosciences, Northwestern University, 2205 Tech Dr, Evanston, IL 60208, USA. Email: erik.andersen@gmail.com

Abstract

Growth rate and body size are complex traits that contribute to the fitness of organisms. The identification of loci that underlie differences in these traits provides insights into the genetic contributions to development. Leveraging *Caenorhabditis elegans* as a tractable metazoan model for quantitative genetics, we can identify genomic regions that underlie differences in growth. We measured postembryonic growth of the laboratory-adapted wild-type strain (N2) and a wild strain from Hawaii (CB4856) and found differences in body size. Using linkage mapping, we identified three distinct quantitative trait loci (QTL) on chromosomes IV, V, and X that are associated with variation in body growth. We further examined these growth-associated quantitative trait loci using chromosome substitution strains and near-isogenic lines and validated the chromosome X quantitative trait loci. In addition, we generated a list of candidate genes for the chromosome X quantitative trait loci. These genes could potentially contribute to differences in animal growth and should be evaluated in subsequent studies. Our work reveals the genetic architecture underlying animal growth variation and highlights the genetic complexity of growth in *Caenorhabditis elegans* natural populations.

Keywords: developmental growth; *Caenorhabditis elegans*; linkage mapping; QTL

Introduction

Precise regulation of final body size is essential to the development and fitness of organisms. Although a larger body size can increase competitive advantages, it also requires added time and nutrients to develop (Hone and Benton 2005). For this reason, mechanisms that control developmental growth rate and ultimate body size are likely under strong natural selection. The robustness and precision with which animal development is choreographed is still not well understood. Developing systems coordinate the organization and interaction among cells, tissues, and organs at high reproducibility even in the presence of genetic and environmental perturbations.

To study the phenomenon of organismal size uniformity, considerable precision and throughput is needed, which can be a challenge when working with multicellular organisms. The nematode *Caenorhabditis elegans* is a powerful model organism to study the developmental growth because it has a quick generation time, produces large numbers of genetically identical offspring, and is easily cultured in controlled laboratory conditions (Wood 1988). Furthermore, *C. elegans* postembryonic development is well characterized and marked by four larval-stage transitions (molts) that separate the *C. elegans* life cycle into five distinct stages: four larval stages (L1–L4) and adult (Singh and Sulston 1978). The timing of these molts determines the completion of stage-specific development (Zaidel-Bar et al. 2010; Monsalve et al. 2011), underscoring the importance of developmental growth regulation in *C. elegans*.

We can leverage *C. elegans* natural genetic diversity to connect phenotypic differences to genetic variants (Evans et al. 2021; Andersen and Rockman 2022). Two particular strains of interest are the laboratory-adapted wild-type strain, N2, and a wild strain from Hawaii, CB4856. The genetic diversity between these two strains was shown to underlie multiple phenotypic differences, including aggregation behavior, life history traits, and gene expression (Evans et al. 2021). Recombinant inbred advanced intercross lines (RIAILs) constructed from crosses between the N2 and CB4856 strains each have unique variants derived from each parental background. Performed at a large scale, these populations of recombinant individuals are a powerful tool to identify genomic regions that are correlated with phenotypic variation. Two sets of strains are available, comprising one panel of 239 N2xCB4856 RIAILs (set 1; Rockman and Kruglyak 2009) and one panel of 359 QX1430xCB4856 RIAILs (set 2; Andersen et al. 2015), which eliminates the phenotypic effects of *npr-1* (Andersen et al. 2014) and reduces the effect of the *peel-1* *zeel-1* (Seidel et al. 2011) incompatibility. Mapping the natural variation underlying phenotypic differences in these RIAILs allows for the dissection of genetic networks involved in important biological processes. Many others have taken this approach to study the genetic underpinnings of complex traits (Evans et al. 2021; Andersen and Rockman 2022).

To characterize the genetic basis for variation in growth in *C. elegans*, we first performed a longitudinal study of postembryonic growth in N2 and CB4856 animals. Although we observed similar

Received: June 29, 2022. Accepted: August 05, 2022

© The Author(s) 2022. Published by Oxford University Press on behalf of Genetics Society of America.

This is an Open Access article distributed under the terms of the Creative Commons Attribution License (<https://creativecommons.org/licenses/by/4.0/>), which permits unrestricted reuse, distribution, and reproduction in any medium, provided the original work is properly cited.

patterns in overall growth dynamics, we also noticed small differences in body size at individual time points across development. To study these differences, we used linkage mapping to identify three distinct quantitative trait loci (QTL) that influence animal growth variation. We further assessed each QTL independently using chromosome substitution strains and near-isogenic lines. Doing so, we validated the chromosome X QTL and identified promising candidate genes that could contribute to the differences in growth between the N2 and CB4856 strains. Our work provides a framework for future studies to investigate the genetic mechanisms controlling developmental growth in natural populations of *C. elegans*.

Materials and methods

Strains

Animals were grown at 20°C on 6 cm plates of modified nematode growth media (NGMA), containing 1% agar and 0.7% agarose seeded with *Escherichia coli* OP50 bacteria. RIAILs used were constructed previously. Set 1 RIAILs were generated using the N2 and CB4856 strains (Rockman and Kruglyak 2009). Set 2 RIAILs were generated using the QX1430 and CB4856 strains (Andersen et al. 2015). The construction of chromosome substitution strains (CSSs) and near-isogenic lines (NILs) used for validation is detailed below. Strains are available upon request.

High-throughput growth assay

Measurements of body size and fluorescence were measured as previously described (Nyaanga et al. 2021). Briefly, the N2 and CB4856 strains were propagated for three generations, bleach-synchronized, and titered at a concentration of one embryo/ μ L into six replicate 500 mL flasks for a final volume of 25 mL. The following day, arrested L1s were fed HB101 food at a final concentration of OD20 in a final flask volume of 100 mL of K medium and HB101 food. Animals were then grown at 20°C with constant shaking. Flasks were sampled each hour beginning one hour after feeding and continuing for 51 consecutive hours. At each hour, animals were sampled from each flask, treated with sodium azide, imaged with an ImageXpress Nano (Molecular Devices, San Jose, CA, USA) and scored using a large-particle flow cytometer (COPAS BIOSORT; Union Biometrica, Holliston, MA, USA). The COPAS BIOSORT platform was used to collect measurements of animal length (TOF) and optical extinction (EXT). Normalized optical extinction (norm.EXT) was previously established as a proxy for animal width. The raw data collected were imported and processed using the *easysorter* R package (Shimko and Andersen 2014). Processing removed nonanimal objects such as bacterial clumps, shed cuticles, and next-generation larval animals from the time-course data using the *mclust* R package (Scrucca et al. 2016). Data for each well were summarized to obtain median well measurements. TOF and norm.EXT data were then converted to microns as previously described (Nyaanga et al. 2022).

High-throughput fitness assay for linkage mapping

For RIAIL phenotyping, we used a high-throughput fitness assay previously described (Andersen et al. 2015). In brief, populations of each strain were propagated on NGMA plates for four generations after which gravid adults were bleach-synchronized and embryos from each strain were aliquoted at a concentration of 25–50 embryos/ μ L into 96-well microtiter plates for a final volume of 50 μ L K medium. The next day, arrested L1s were fed HB101 bacterial lysate (Pennsylvania State University Shared

Fermentation Facility, State College, PA, USA; García-González et al. 2017) at a final concentration of 5 mg/mL in K medium and grown to the L4 larval stage for 48 h at 20°C with constant shaking. Animals were then sorted using a COPAS BIOSORT platform during which time animal length and width were collected. Measurements collected by the COPAS BIOSORT were processed and analyzed using the *easysorter* R package (Shimko and Andersen 2014). Well populations of recombinant strains that contained more than 100 or fewer than three individuals were removed from further processing, resulting in an average of 25 independent replicate wells per strain. Differences among strains tested on different days were controlled using a linear model ($animal_size \sim experiment_date$). In this way, we address only the differences among strains caused by growth and the day-to-day experimental variance is controlled. These residual values are used for plotting.

Linkage mapping

A total of 291 RIAILs (set 2 RIAILs) were phenotyped using the high-throughput assay described above. Linkage mapping was performed for body-size traits using the R package *linkagemapping* (www.github.com/AndersenLab/linkagemapping) as previously described (Brady et al. 2019). The genotypic data and residual phenotypic data were merged using the *merge_pheno* function with the argument $set = 2$. QTL were detected using the *fsearch* function. This function calculates the logarithm of the odds (LOD) scores for each genetic marker and each trait as $-\ln(1 - R^2) / 2\ln(10)$ where R is the Pearson correlation coefficient between the RIAIL genotypes at the marker and trait values (Bloom et al. 2013). A significance threshold based on a 5% genome-wide error rate was calculated by permuting the phenotypic values of each RIAIL 1,000 times. QTL were identified as the marker with the highest LOD score above the significance threshold. This marker was then integrated into the model as a cofactor and mapping was repeated iteratively until no further significant QTL were identified. Finally, the *annotate_lds* function was used to calculate the effect size of each QTL. 95% confidence intervals were defined by a 1.5-LOD drop from the peak marker.

Generation of CSSs and NILs

CSSs were generated from a cross of the N2 and CB4856 strains. These strains were crossed and heterozygous hermaphrodite progeny were mated to each parental genotype for four generations followed by three generations of selfing to ensure homozygosity of the genome. For each cross, PCR amplicons for insertion–deletions (indels) on the left and right sides of chromosomes IV and V were used to confirm progeny genotypes and select nonrecombinants within the introgressed region (Supplementary Text 1). CSSs were whole-genome sequenced to confirm their genotypes.

NILs were generated as previously described (Zdraljevic et al. 2017, 2019; Evans et al. 2018; Brady et al. 2019) either by backcrossing a selected RIAIL or NIL for six generations or *de novo* by crossing the parental strains N2 and CB4856 to create a heterozygous individual that was then backcrossed for six generations. PCR amplicons for indel variants were used to track the genomic interval (Supplementary Text 1). NILs were whole-genome sequenced to verify introgressions.

Statistical analysis of CSS and NIL results

Growth dynamics for CSSs were tested using a modified version of the high-throughput fitness assay for linkage mapping. Animals were propagated on NGMA plates for two generations

before gravid adults were bleach-synchronized and embryos from each strain were aliquoted at a concentration of one embryo/ μL into 12-well, flat bottom culture plates. After three days, gravid adults were bleach-synchronized and embryos were titered into 96-well microtiter plates at a concentration of 50 embryos/ μL for a final volume of 50 μL K medium. The next day, arrested L1s were fed HB101 live bacterial food at a final concentration of OD20. Animals were grown for 48 h at 20°C with constant shaking and then scored using the COPAS BIOSORT platform as before. The raw data collected were again imported and processed using the *easysorter* R package (Shimko and Andersen 2014). Processing removed non-animal objects such as bacterial clumps, shed cuticles, and next-generation larval animals from the time-course data using the *mclust* R package (Scrucca et al. 2016). Complete pairwise strain comparisons were performed using the *TukeyHSD* function (R Core Team and Others 2013) on an ANOVA model with the formula *phenotype* ~ *strain*. A *P*-value of <0.05 was used as a threshold for statistical significance. Recapitulation was defined by the significance and direction of effect the CSS or NIL had compared to the parental strains.

Results

Growth dynamics of the N2 and CB4856 strains

To precisely evaluate *C. elegans* growth dynamics, we previously developed a high-throughput growth assay that integrates image-based and flow-based devices to quantify the growth of thousands of animals over developmental time (Nyaanga et al. 2021). We used this assay to collect body-size measurements of N2 and CB4856 animals over the course of larval development from the L1 stage through the L4 stage. Briefly, populations of 100,000 animals were cultured in flasks in triplicate for each strain. Every hour after feeding, we sampled approximately 300 animals from each flask, collected images, and measured length (TOF) and width (norm.EXT) of sampled animals using the COPAS BIOSORT platform (Supplementary Figs. 1 and 2 and Supplementary File 1). From these raw body-size measurements, we removed non-animal objects using model-based clustering and generated summary statistics to study population changes (Supplementary Figs. 3 and 4, Supplementary File 2, see *Materials and Methods*). Here, we report the mean length and width of animals over 51 consecutive developmental time points (Fig. 1). Overall, we observed little divergence in the growth behavior between the two strains. As previously reported, we detected continuous growth punctuated by periods of discontinuous growth rate, resulting in visible shifts in length and width over time. Although growth behavior is consistent in both N2 and CB4856 animals, we observed significant differences in animal length and width at individual time points, particularly early in development (Supplementary Fig. 5). As animals age, we identify fewer time points with significant differences likely because of increased variability in body size across the population. We find that in all instances where we observed a significant difference in animal length, animals from the N2 strain were consistently longer than animals from the CB4856 strain. However, this result was not observed in animal width as we observed time points where the CB4856 strain was wider than the N2 strain and other timepoints with the opposite result.

Identification of QTL underlying variation in growth

As a complex trait, developmental growth is likely influenced by many genes as well as the interactions among them. To investigate the genetic basis of differences in growth, we assessed the development of a panel of 291 RIALs derived from a cross between the N2 and CB4856 strains (set 2 RIALs, see *Materials and Methods*). In lieu of collecting measurements throughout development, we used body size as a convenient proxy for developmental progression, where fast growth corresponds to large size and slow growth corresponds to small size. After 48 h post-L1 arrest, we collected measurements of length and width using a high-throughput fitness assay, and removed wells containing more than 100 or fewer than three animals from downstream processing (Supplementary File 3, see *Materials and Methods*). Doing so, we observed a distribution of both mean length (Fig. 2a) and mean width (Fig. 2d) among the RIALs, indicating that growth rate varies in the strain population. Next, we mapped body length and width separately and obtained three significant QTL (Fig. 2, b and e and Supplementary File 4). The length-associated QTL on the center of chromosome IV and the width-associated QTL on the center of chromosome V independently explain approximately 5% of the phenotypic variation among the RIALs. The third QTL on the right arm of chromosome X explains slightly more variation at 8.6% (Table 1). Notably, not only did we find distinct QTL for growth in length and growth in width, we also observed QTL with opposite effects on body shape growth. Strains with the N2 allele at the chromosome IV QTL grew longer than strains with the CB4856 allele at this QTL (Fig. 2c). By contrast, strains with the CB4856 alleles at the chromosome V and X QTL grew wider than strains with the N2 allele at these QTL (Fig. 2f). The identification of distinct QTL for growth in length vs. growth in width indicates that body shape is influenced by multiple genetic mechanisms. In addition, we scanned the genome for interactions between pairs of genomic markers that could affect the phenotypic distribution of length or width in the RIALs and identified no significant interactions (Supplementary Figs. 6 and 7). These data suggest that the three identified loci contain variants that uniquely influence growth rate along multiple axes, where each locus independently affects the longitudinal or circumferential growth of animals.

Validation of loci associated with differences in animal growth

To validate whether genetic variation between the N2 and CB4856 strains contributes to differences in animal growth, we generated CSSs for chromosomes IV and V in which the entire chromosome from the N2 strain was introgressed into the CB4856 genetic background and vice versa. We also constructed reciprocal NILs for the chromosome IV, V, and X QTL (Supplementary Files 5 and 6). These NILs contain a small genomic segment derived from one parent strain introgressed into the genetic background of the other parent strain. We then measured the length and width of animals after 48 h of growth and calculated statistical significance in a pairwise manner for each strain (Supplementary Files 7 and 8, see *Materials and Methods*). For the chromosome IV and V QTL, we were unable to recapitulate the results observed in the linkage mapping (Supplementary Figs. 8 and 9 and Supplementary File 9). These two QTL each explain only 5% of the total phenotypic variation among the RIALs and have the smallest effect sizes among the three detected QTL (Table 1). The inability to validate these QTL suggests a complex

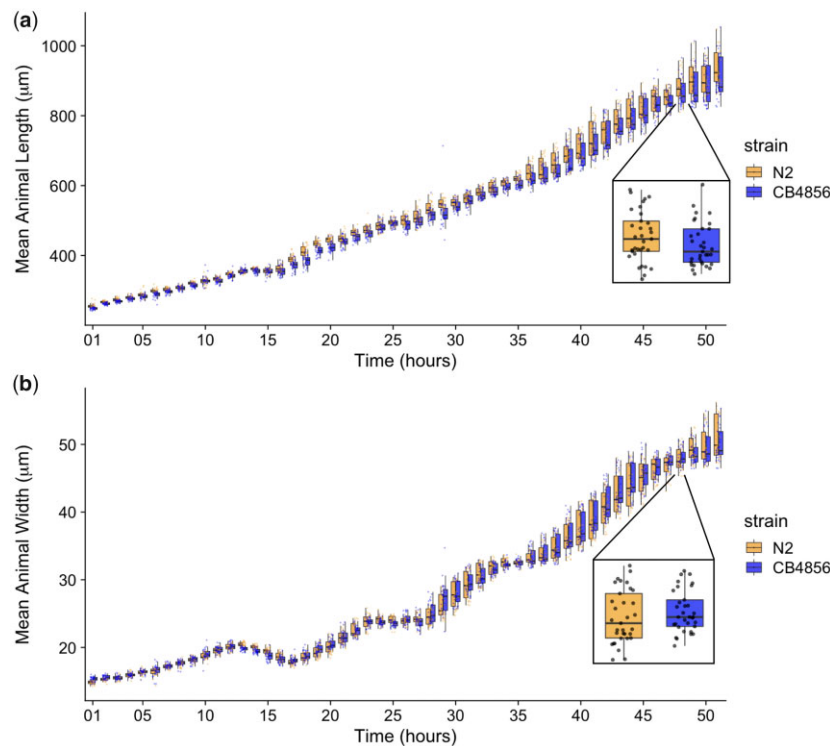


Fig. 1. Quantitative measurements of growth for N2 and CB4856 animals. Tukey boxplots of mean length (a) and mean width (b) for the N2 (orange) and CB4856 (blue) strains over developmental time. The horizontal line in the middle of the box is the median, and the box denotes the 25th to 75th quantiles of the data. The vertical line represents the 1.5 interquartile range. Inset plots magnify mean animal size measurements from hour 48. Each point corresponds to the mean length or mean width of a population of animals in each well.

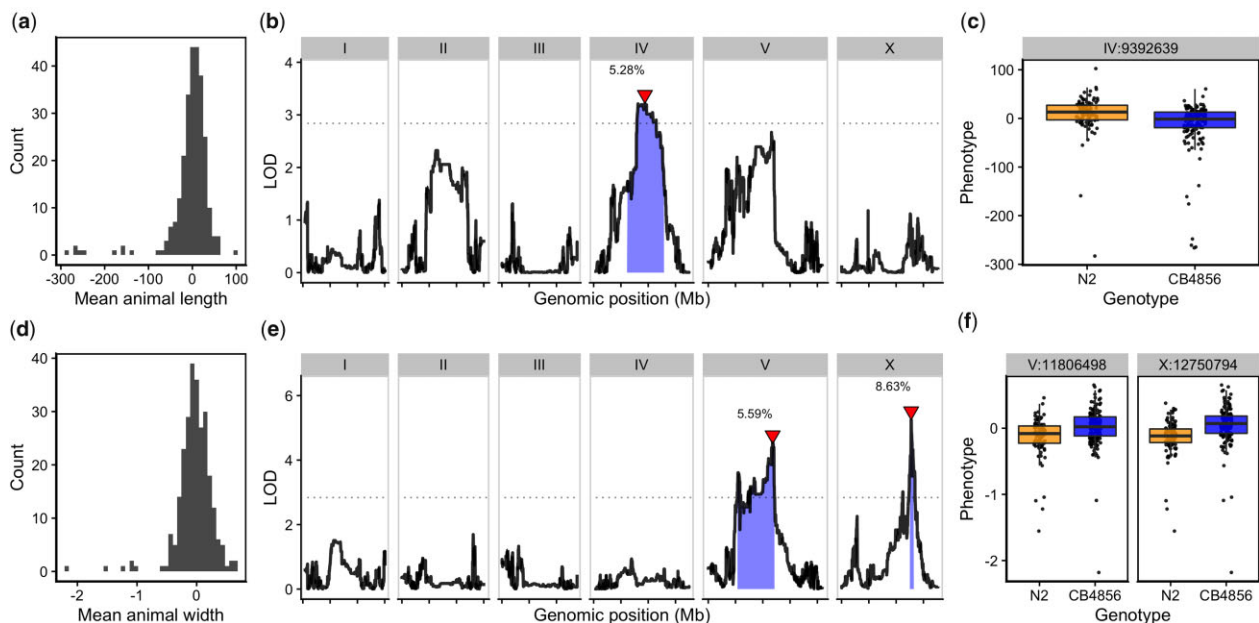


Fig. 2. Linkage mapping identifies 3 QTL associated with body growth. Histogram of residual mean body length (a) and mean body width (d) of the RIAIL population. b, e) Linkage mapping results for mean body length or mean body width are shown with genomic position (x-axis) plotted against the LOD score (y-axis). X-axis tick marks denote every 5 Mb. Significant QTL are denoted by a red triangle at the peak marker, and blue shading shows the 95% confidence interval around the peak marker. The 5% genome-wide error rate LOD threshold is represented as a dashed horizontal line. The percentage of the total phenotypic variance in the RIAIL population that is explained by each QTL is shown above the peak marker. c, f) Tukey box plots show the residual mean length or width (y-axis) of RIAILs split by genotype at the marker with the maximum LOD score (x-axis). Populations of recombinant strains were grown in independent wells. Each point corresponds to the mean value calculated from each assayed well. Boxes for data from strains with the N2 allele are colored orange, and boxes for data from strains with the CB4856 allele are shown in blue.

Table 1. Body growth QTL.

Trait	Chromosome	Interval (bp)	Peak	LOD	Variance explained (%)	Effect size
Length	IV	6,211,685–12,868,784	9,392,639	3.22	5.28	−0.229
Width	V	5,371,124–12,112,105	11,806,498	4.54	5.59	0.236
Width	X	12,565,734–13,173,080	12,750,794	5.25	8.63	0.293

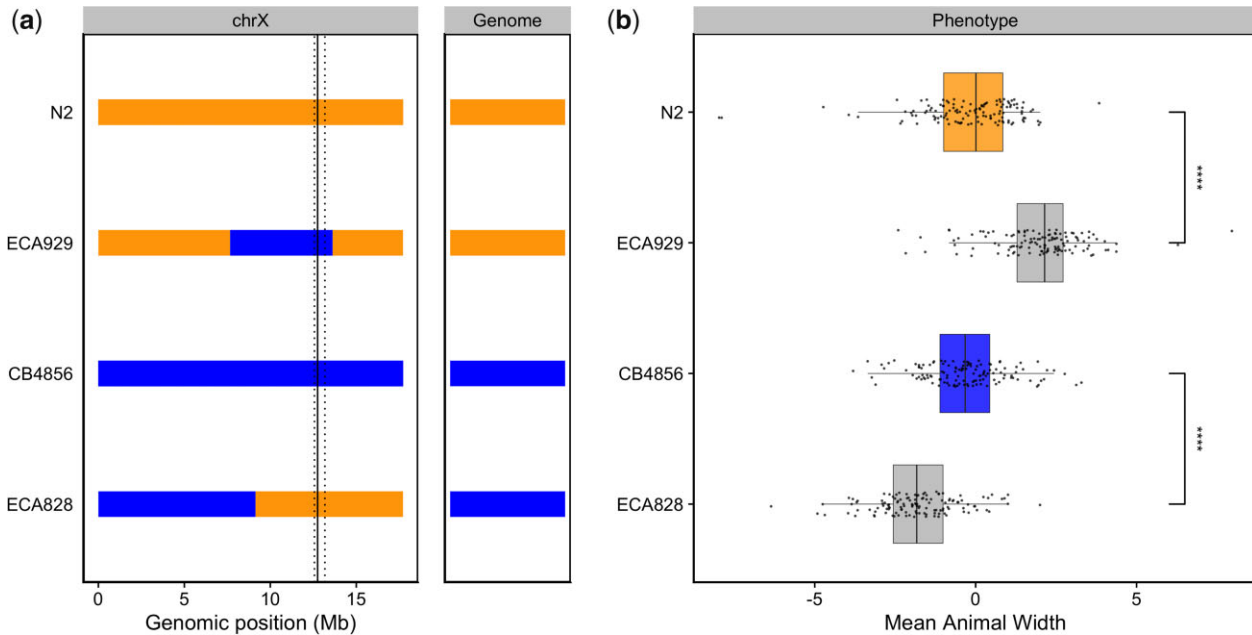


Fig. 3. NILs validated the chromosome X QTL. a) Strain genotypes are displayed as colored rectangles (N2: orange, CB4856: blue) for chromosome X (left) and in general for the rest of the chromosomes (right). The solid vertical line represents the peak marker of the QTL. The dashed vertical lines represent the confidence interval. b) Residual mean animal width (x-axis) is plotted as Tukey box plots against strain (y-axis). Each point corresponds to the mean width of a population of animals from each well. The boxes for the parental strains are colored: N2, orange; CB4856, blue. Statistical significance was calculated by Tukey's HSD (****P-value < 0.0001).

genetic architecture that cannot be explained by isolating these loci using CSSs and NILs, or a lack of power to detect differences driven by these QTL in the CSSs and NILs. By contrast, we successfully validated the chromosome X QTL by observing that genotype significantly contributed to differences in the width growth of NILs (Fig. 3 and Supplementary File 10). The strain with the CB4856 allele on chromosome X crossed into the N2 genetic background grew significantly wider than the N2 strain (Tukey's HSD, P -value = $1.29e^{-10}$). Similarly, the strain with the N2 chromosome X region introgressed into the CB4856 genetic background grew significantly thinner than the CB4856 strain (Tukey's HSD, P -value = $1.29e^{-10}$). These results confirmed that genetic variation between the N2 and CB4856 strains on chromosome X contributes to the difference in body width growth between these strains.

Identification of candidate genes in the chromosome X QTL

To identify candidate genes that could underlie variation in body width growth, we investigated the genes in the chromosome X interval in the N2 strain. We found 151 genes present in this interval and eliminated 96 genes that had no genetic variation in the CB4856 strain (Table 2 and Supplementary File 11). Of the remaining 55 genes, 18 have genetic variation in the amino-acid sequence of a protein (protein-coding variation) and 34 have genetic variation that is not protein-coding (noncoding variation).

Table 2. Genes in QTL interval for chromosome X.

No. variation ^a	Protein-coding variation and/or eQTL ^b	Noncoding variation ^c	Other eQTL that map to interval ^d	Total
96	21	34	17	168

- ^a Genes within genomic interval with no genetic variation.
^b Genes within genomic interval with protein-coding variation and/or an eQTL that maps to this interval.
^c Genes within genomic interval with noncoding variation and no eQTL that maps to this interval.
^d Genes outside genomic interval with eQTL that maps to this interval.

However, protein-coding variation is just one way in which genetic variation can cause phenotypic variation. We also considered instances where genetic variation causes a change in gene expression. Using an expression QTL (eQTL) dataset that mapped expression differences in another panel of RIALs (set 1) derived from N2 and CB4856 (Rockman and Kruglyak 2009; Evans and Andersen 2020), we identified five genes with eQTL that map to our region of interest. In addition, we found 17 other genes outside this genomic interval with eQTL that map to this interval, resulting in a total of 72 candidate genes, none of which are located within a hyper-divergent region (Lee et al. 2021).

To further narrow our list of genes, we inspected the functional descriptions and gene ontology (GO) annotations for the 72 candidate genes. When considering the 21 genes with protein-

coding variation and/or eQTL, one candidate (*ppk-3*) stood out. Phosphatidylinositol phosphate kinase 3 (*ppk-3*) is an ortholog of the mammalian PIKfyve. These kinases play important roles in cell communication and membrane trafficking (Gillooly et al. 2001). Notably, mutations in *ppk-3* are responsible for a range of developmental defects, including embryonic lethality, developmental arrest, and larval growth delay (Nicot et al. 2006). Investigating the sequence read alignments of the N2 and CB4856 strains at the *ppk-3* locus using the Variant Browser on CeNDR (Cook et al. 2017), we observed a missense variant in the second exon predicted to encode a serine-to-threonine substitution (S43T). Although this variant is not in a predicted functional domain, it could alter protein function thereby contributing to the observed phenotypic difference. Aside from *ppk-3*, we identified two additional candidate genes when assessing the functional description for the 34 genes with noncoding genetic variation. The first, *nhr-25*, encodes a nuclear hormone receptor orthologous to Ftz-F1 in *Drosophila* and is required for proper molting and developmental control (Asahina et al. 2000). We observed a splice-site variant in the *nhr-25* locus that could disrupt proper RNA splicing. Interestingly, disruption of *nhr-25* often causes embryonic arrest; however, mutants that survive hatching display a squat body stature (Dpy phenotype), suggesting that *nhr-25* could play a role in body size and shape (Gissendanner and Sluder 2000). The second, *bcat-1*, encodes a branched-chain amino acid aminotransferase that was shown to be required for normal embryonic and larval development (Maeda et al. 2001). In the *bcat-1* locus, we found a variant in an intron and in the 3'-untranslated region. Together, these results suggest that one or more genes on chromosome X are candidates that need additional study to explain the variation that we observe in animal growth.

Discussion

Here, we investigated the larval growth of N2 and CB4856 animals from the L1 stage to the L4 stage. Although we observed similarities in the patterns of growth, we also saw differences in the size of animals across developmental time. We used linkage mapping to investigate these differences and identified three small-effect QTL associated with variation in body growth. Two QTL underlie variation in width growth, and a single nonoverlapping QTL contributes to differences in length growth. Using NILs, we validated the width-associated QTL on chromosome X and identified candidate genes that could underlie variation in the growth of width. Taken together, our results demonstrate the power of leveraging natural genetic variation to examine the genetic architecture of complex traits such as developmental growth.

A complex genetic architecture underlies differences in body growth

As a complex life history trait, developmental growth could be influenced by several loci (Houle 1992). In this study, we report three growth-associated QTL. Strikingly, we find loci that decouple components of body size, revealing a complex genetic system that influences growth along different axes of the body. Evidence for genetically separate modules underlying distinct aspects of a single trait has been observed in studies of *C. elegans* behavioral patterns where linkage mapping studies using a panel of RIALLs (set 1; Rockman and Kruglyak 2009) identified distinct loci underlying separate aspects of a response to thermal stimuli (Ghosh et al. 2015). Here, we identify distinct QTL for growth in length and growth in width, suggesting that different genetic

mechanisms control animal growth along the length vs. width directions. This finding is particularly interesting given the differences in general growth dynamics of length compared to width that we found here (Fig. 1) and previously (Nyaanga et al. 2021) observed as a simultaneous increase in length and a decrease in width at the transition between larval stages.

The results of the linkage mapping experiment identified two broad peaks on chromosomes IV and V associated with length and width growth, respectively, as well as a narrow peak on chromosome X for width growth. Notably, of these three detected QTL, only one (chromosome V) has a confidence interval that includes a gene characterized to have a laboratory-derived allele in N2 (*glb-5*) (Sterken et al. 2015). Although it is possible that *glb-5* contributes to some of the phenotypic variation that we observe, it is also likely that independent natural variants are contributing to the observed effect. Furthermore, although we successfully validated the width-associated QTL on chromosome X (Fig. 3), we were unable to validate the QTL on chromosomes IV and V (Supplementary Figs. 8 and 9). Our inability to recapitulate the results observed in the linkage mapping might be driven by several factors. First, many loci spread across the genome could underlie variation in body growth. Under this polygenic model, any region can harbor variants driving our observed phenotypic difference through additive and/or nonadditive effects. The contribution of polygenicity to phenotypic variance has previously been explored in *C. elegans*. Studies of fertility and body size in the *C. elegans* multiparental experimental evolution panel found that a significant fraction of phenotypic variance, nearly 40% for fertility, can be explained by polygenicity (Noble et al. 2017). Second, the intervals could contain QTL of opposing effects, making it difficult to recapitulate the results observed in the mapping using NILs. Notably, researchers have observed patterns of polygeny and antagonistic-effect loci when investigating *C. elegans* growth and reproduction in nickel stress (Bernstein et al. 2019). Third, it is possible that the QTL effects are smaller than 5% and we are underpowered to detect differences driven by these QTL in the CSSs and NILs.

Candidate genes for variation in body growth

Genetic variants underlying complex traits are often elusive (Rockman 2012; Evans et al. 2021). Ultimately, when searching for QTL, we aim to identify genes contributing to the variation in phenotypes among individuals. Here, we identified candidate genes located in the interval of the chromosome X QTL (Table 2 and Supplementary File 11). However, complex traits, such as body growth, are likely affected by many genes. In the laboratory strain of *C. elegans*, we know many loci that quantitatively affect body size and shape. Mutations in these genes span various classes, including abnormal pharyngeal pumping (*Eat*), egg-laying defective (*Egl*), uncoordinated (*Unc*), abnormal dauer formation (*Daf*), and several cuticle and body shape classes (*Dpy*, *Lon*, *Sma*, *Rol*, *Sqt*) (Mörck and Pilon 2006; So et al. 2011; Cho et al. 2021). The polygenic nature of complex traits is a recognized barrier in identifying the genes contributing to phenotypic variation in a population (Boyle et al. 2017; Bernstein et al. 2019). However, we believe that molecular analysis of loci that underlie variation in development-associated traits is essential to deciphering the influence of natural genetic variation on *C. elegans* growth.

Comparison with previous QTL studies of *C. elegans* growth

Our mapping results both recapitulate and expand upon previous QTL studies of growth in *C. elegans*. Previously, the median body

length of mixed-stage animals was mapped using the same panel of RIAILs (set 2) (Andersen *et al.* 2015). A single small-effect (5.7%) QTL in the center of chromosome IV was found, consistent with our findings. Also, in this study, the authors mapped median body width (norm.EXT) to three QTL on chromosomes III, IV, and X. We detected an overlapping genomic region on chromosome X in our current study. The failure to recapitulate the other QTL is likely caused by differences in experimental conditions as the previous study measured mixed-stage animals and we focused on synchronized L4 animals. In addition, others have mapped variation in animal length for a collection of N2xCB4856 introgression lines at 48 h after L1 arrest (Snoek *et al.* 2014). Here, investigators found five separate QTL on chromosome IV affecting body size. This result suggests the presence of several independent loci on chromosome IV each contributing to variation in length growth. Further investigation is necessary to determine whether the overlapping genomic region detected in our current study is in fact a separate locus that independently contributes to variation in animal length. Most recently, a group using a N2xCB4856 RIL population identified 18 QTL influencing various body-size traits at a range of temperatures, with the majority clustering on chromosome X (Maulana *et al.* 2022). This work not only demonstrates the genetic complexity underlying body-size phenotypes but also suggests the presence of coregulatory loci underlying plasticity. *C. elegans* gives investigators a powerful system to understand the genetic mechanisms that shape growth and environmental sensitivity in natural populations.

Data availability

The authors state that all data necessary to confirm the conclusions of this work are within the text, figures, and supporting information files. [Supplementary Files 1–11](#), [Supplementary Text 1](#), and code for analysis and generation of figures and tables are available on GitHub (<https://github.com/AndersenLab/N2CB-growth-manuscript>).

[Supplemental material](#) is available at G3 online.

Acknowledgments

We thank Sophia Gibson and Gaotian Zhang for their help sampling animals during the 51 h growth assay.

Author contributions

JN: conceptualization, investigation, methodology, formal analysis, writing—original draft, and writing—review and editing. ECA: conceptualization, funding acquisition, investigation, supervision, and writing—review and editing.

Funding

For this work, JN and ECA received support from the NSF-Simons Center for Quantitative Biology at Northwestern University (awards Simons Foundation/SFARI 597491-RWC and the National Science Foundation 1764421).

Conflicts of interest

None declared.

Literature cited

- Andersen EC, Bloom JS, Gerke JP, Kruglyak L. A variant in the neuropeptide receptor *npr-1* is a major determinant of *Caenorhabditis elegans* growth and physiology. *PLoS Genet.* 2014;10(2):e1004156.
- Andersen EC, Rockman MV. Natural genetic variation as a tool for discovery in *Caenorhabditis* nematodes. *Genetics.* 2022;220(1):iyab156.
- Andersen EC, Shimko TC, Crissman JR, Ghosh R, Bloom JS, Seidel HS, Gerke JP, Kruglyak L. A powerful new quantitative genetics platform, combining *Caenorhabditis elegans* high-throughput fitness assays with a large collection of recombinant strains. *G3 (Bethesda).* 2015;5(5):911–920.
- Asahina M, Ishihara T, Jindra M, Kohara Y, Katsura I, Hirose S. The conserved nuclear receptor Ftz-F1 is required for embryogenesis, moulting and reproduction in *Caenorhabditis elegans*. *Genes Cells.* 2000;5(9):711–723.
- Bernstein MR, Zdraljevic S, Andersen EC, Rockman MV. Tightly linked antagonistic-effect loci underlie polygenic phenotypic variation in *C. elegans*. *Evol Lett.* 2019;3(5):462–473.
- Bloom JS, Ehrenreich IM, Loo WT, Lite T-LV, Kruglyak L. Finding the sources of missing heritability in a yeast cross. *Nature.* 2013;494(7436):234–237.
- Boyle EA, Li YI, Pritchard JK. An expanded view of complex traits: from polygenic to omnigenic. *Cell.* 2017;169(7):1177–1186.
- Brady SC, Zdraljevic S, Bisaga KW, Tanny RE, Cook DE, Lee D, Wang Y, Andersen EC. A novel gene underlies bleomycin-response variation in *Caenorhabditis elegans*. *Genetics.* 2019;212(4):1453–1468.
- Cho JY, Choi T-W, Kim SH, Ahn J, Lee S-K. Morphological characterization of small, dumpy, and long phenotypes in *Caenorhabditis elegans*. *Mol Cells.* 2021;44(3):160–167.
- Cook DE, Zdraljevic S, Roberts JP, Andersen EC. CeNDR, the *Caenorhabditis elegans* natural diversity resource. *Nucleic Acids Res.* 2017;45(D1):D650–D657.
- Evans KS, Andersen EC. The gene *scb-1* underlies variation in *Caenorhabditis elegans* chemotherapeutic responses. *G3 (Bethesda).* 2020;10(7):2353–2364.
- Evans KS, Brady SC, Bloom JS, Tanny RE, Cook DE, Giuliani SE, Hippleheuser SW, Zamanian M, Andersen EC. Shared genomic regions underlie natural variation in diverse toxin responses. *Genetics.* 2018;210(4):1509–1525.
- Evans KS, van Wijk MH, McGrath PT, Andersen EC, Sterken MG. From QTL to gene: *C. elegans* facilitates discoveries of the genetic mechanisms underlying natural variation. *Trends Genet.* 2021;37(10):933–947.
- García-González AP, Ritter AD, Shrestha S, Andersen EC, Yilmaz LS, Walhout AJM. Bacterial metabolism affects the *C. elegans* response to cancer chemotherapeutics. *Cell.* 2017;169(3):431–441.e8.
- Ghosh R, Bloom JS, Mohammadi A, Schumer ME, Andolfatto P, Ryu W, Kruglyak L. Genetics of intraspecies variation in avoidance behavior induced by a thermal stimulus in *Caenorhabditis elegans*. *Genetics.* 2015;200(4):1327–1339.
- Gillooly DJ, Simonsen A, Stenmark H. Cellular functions of phosphatidylinositol 3-phosphate and FYVE domain proteins. *Biochem J.* 2001;355(Pt 2):249–258.
- Gissendanner CR, Sluder AE. *nhr-25*, the *Caenorhabditis elegans* ortholog of *ftz-f1*, is required for epidermal and somatic gonad development. *Dev Biol.* 2000;221(1):259–272.
- Hone DWE, Benton MJ. The evolution of large size: how does Cope's Rule work? *Trends Ecol Evol.* 2005;20(1):4–6.
- Houle D. Comparing evolvability and variability of quantitative traits. *Genetics.* 1992;130(1):195–204.

- Lee D, Zdraljjevic S, Stevens L, Wang Y, Tanny RE, Crombie TA, Cook DE, Webster AK, Chirakar R, Baugh LR, et al. Balancing selection maintains hyper-divergent haplotypes in *Caenorhabditis elegans*. *Nat Ecol Evol*. 2021;5(6):794–807.
- Maeda I, Kohara Y, Yamamoto M, Sugimoto A. Large-scale analysis of gene function in *Caenorhabditis elegans* by high-throughput RNAi. *Curr Biol*. 2001;11(3):171–176.
- Maulana MI, Riksen JAG, Snoek BL, Kammenga JE, Sterken MG. The genetic architecture underlying body-size traits plasticity over different temperatures and developmental stages in *Caenorhabditis elegans*. *Heredity*. 2022;128(5):313–324.
- Monsalve GC, Van Buskirk C, Frand AR. LIN-42/PERIOD controls cyclical and developmental progression of *C. elegans* molts. *Curr Biol*. 2011;21(24):2033–2045.
- Mörck C, Pilon M. *C. elegans* feeding defective mutants have shorter body lengths and increased autophagy. *BMC Dev Biol*. 2006;6:39.
- Nicot A-S, Fares H, Payrastrre B, Chisholm AD, Labouesse M, Laporte J. The phosphoinositide kinase PIKfyve/Fab1p regulates terminal lysosome maturation in *Caenorhabditis elegans*. *Mol Biol Cell*. 2006;17(7):3062–3074.
- Noble LM, Chelo I, Guzella T, Afonso B, Riccardi DD, Ammerman P, Dayarian A, Carvalho S, Crist A, Pino-Querido A, et al. Polygenicity and epistasis underlie fitness-proximal traits in the *Caenorhabditis elegans* multiparental experimental evolution (CeMEE) panel. *Genetics*. 2017;207(4):1663–1685.
- Nyaanga J, Goss C, Zhang G, Ahmed HN, Andersen EJ, Miller IR, Rozenich JK, Swarthout IL, Vaughn JA, Mangan NM, et al. Changes in body shape implicate cuticle stretch in *C. elegans* growth control. *Cells Dev*. 2022;170:203780.
- Nyaanga J, Goss C, Zhang G, Ahmed HN, Andersen EJ, Miller IR, Rozenich JK, Swarthout IL, Vaughn JA, Andersen EC, et al. Highly scaled measurements of *C. elegans* development suggest that physical constraints guide growth trajectories and animal shape. *bioRxiv* 2021.04.01.438121, 2021.
- R Core Team and Others. *R: A Language and Environment for Statistical Computing*; 2013.
- Rockman MV. The QTN program and the alleles that matter for evolution: all that's gold does not glitter. *Evolution*. 2012;66(1):1–17.
- Rockman MV, Kruglyak L. Recombinational landscape and population genomics of *Caenorhabditis elegans*. *PLoS Genet*. 2009;5(3):e1000419.
- Scrucca L, Fop M, Murphy TB, Raftery AE. mclust 5: clustering, classification and density estimation using Gaussian finite mixture models. *R J*. 2016;8(1):289–317.
- Seidel HS, Aillion M, Li J, van Oudenaarden A, Rockman MV, Kruglyak L. A novel sperm-delivered toxin causes late-stage embryo lethality and transmission ratio distortion in *C. elegans*. *PLoS Biol*. 2011;9(7):e1001115.
- Shimko TC, Andersen EC. COPASutils: an R package for reading, processing, and visualizing data from COPAS large-particle flow cytometers. *PLoS One*. 2014;9(10):e1111090.
- Singh RN, Sulston JE. Some observations on moulting in *Caenorhabditis elegans*. *Nematologica*. 1978;24(1):63–71.
- Snoek LB, Orbidans HE, Stastna JJ, Aartse A, Rodriguez M, Riksen JAG, Kammenga JE, Harvey SC. Widespread genomic incompatibilities in *Caenorhabditis elegans*. *G3 (Bethesda)*. 2014;4(10):1813–1823.
- So S, Miyahara K, Ohshima Y. Control of body size in *C. elegans* dependent on food and insulin/IGF-1 signal. *Genes Cells*. 2011;16(6):639–651.
- Sterken MG, Snoek LB, Kammenga JE, Andersen EC. The laboratory domestication of *Caenorhabditis elegans*. *Trends Genet*. 2015;31(5):224–231.
- Wood WB. *The Nematode Caenorhabditis elegans*. Cold Spring Harbor Laboratory; 1988. https://books.google.com/books/about/The_Nematode_Caenorhabditis_Elegans.html?id=S1fwAAAAMAAJ
- Zaidel-Bar R, Miller S, Kaminsky R, Broday L. Molting-specific down-regulation of *C. elegans* body-wall muscle attachment sites: the role of RNF-5 E3 ligase. *Biochem Biophys Res Commun*. 2010;395(4):509–514.
- Zdraljjevic S, Fox BW, Strand C, Panda O, Tenjo FJ, Brady SC, Crombie TA, Doench JG, Schroeder FC, Andersen EC, et al. Natural variation in *C. elegans* arsenic toxicity is explained by differences in branched chain amino acid metabolism. *eLife*. 2019;8. <https://doi.org/10.7554/eLife.40260>
- Zdraljjevic S, Strand C, Seidel HS, Cook DE, Doench JG, Andersen EC. Natural variation in a single amino acid substitution underlies physiological responses to topoisomerase II poisons. *PLoS Genet*. 2017;13(7):e1006891.

Communicating editor: K. Gunsalus